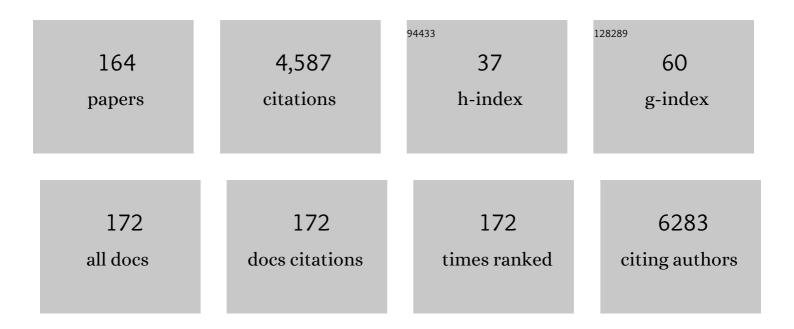
List of Publications by Year in descending order

Source: https://exaly.com/author-pdf/4314174/publications.pdf Version: 2024-02-01



ANNE POIVAINEN

#	Article	IF	CITATIONS
1	Exploiting Glutamine Consumption in Atherosclerotic Lesions by Positron Emission Tomography Tracer (2S,4R)-4-18F-Fluoroglutamine. Frontiers in Immunology, 2022, 13, 821423.	4.8	1
2	Positron Emission Tomography in Research. Methods in Molecular Biology, 2022, 2419, 825-839.	0.9	0
3	PET imaging of bacteria. , 2022, , .		0
4	⁶⁸ Ga-Citrate Positron Emission Tomography of Healthy Men: Whole-Body Biodistribution Kinetics and Radiation Dose Estimates. Journal of Nuclear Medicine, 2022, , jnumed.122.263884.	5.0	0
5	Assessment of myocardial viability with [150]water PET: A validation study in experimental myocardial infarction. Journal of Nuclear Cardiology, 2021, 28, 1271-1280.	2.1	19
6	18F-FDG positron emission tomography/computed tomography of cardiac implantable electronic device infections. Journal of Nuclear Cardiology, 2021, 28, 2992-3003.	2.1	13
7	The circadian gene Cryptochrome 2 influences stressâ€induced brain activity and depressiveâ€like behavior in mice. Genes, Brain and Behavior, 2021, 20, e12708.	2.2	10
8	First-in-Humans Study of ⁶⁸ Ga-DOTA-Siglec-9, a PET Ligand Targeting Vascular Adhesion Protein 1. Journal of Nuclear Medicine, 2021, 62, 577-583.	5.0	13
9	Efficacy and tolerability of folate-aminopterin therapy in a rat focal model of multiple sclerosis. Journal of Neuroinflammation, 2021, 18, 30.	7.2	6
10	Docetaxel chemotherapy response in PC3 prostate cancer mouse model detected by rotating frame relaxations and water diffusion. NMR in Biomedicine, 2021, 34, e4483.	2.8	1
11	Evaluation of glucagon-like peptide-1 receptor expression in nondiabetic and diabetic atherosclerotic mice using PET tracer ⁶⁸ Ga-NODAGA-exendin-4. American Journal of Physiology - Endocrinology and Metabolism, 2021, 320, E989-E998.	3.5	5
12	Statistical Evaluation of Different Mathematical Models for Diffusion Weighted Imaging of Prostate Cancer Xenografts in Mice. Frontiers in Oncology, 2021, 11, 583921.	2.8	1
13	Controlled Monofunctionalization of Molecular Spherical Nucleic Acids on a Buckminster Fullerene Core. Bioconjugate Chemistry, 2021, 32, 1130-1138.	3.6	9
14	Association between [68Ca]NODAGA-RGDyK uptake and dynamics of angiogenesis in a human cell-based 3D model. Molecular Biology Reports, 2021, 48, 5347-5353.	2.3	1
15	Factors driving endothelial cell state changes in atherosclerosis. Atherosclerosis, 2021, 331, e63.	0.8	0
16	Exploiting glutamine consumption in inflamed atherosclerotic lesions by positron emission tomography tracer (2S, 4R)-4-[18F]Fluoroglutamine. Atherosclerosis, 2021, 331, e31-e32.	0.8	0
17	Adipose tissue exposed to high fat diet affects extracellular matrix genes in the mesenchymal stem cell population. Atherosclerosis, 2021, 331, e144.	0.8	0

18

Role of Brown and Beige Adipose Tissues in Seasonal Adaptation in the Raccoon Dog (Nyctereutes) Tj ETQq0 0 0 rg β_1 /Overlock 10 Tf 50 Advector 10 Tf 50 A

#	Article	IF	CITATIONS
19	Coronary, aortic and carotid artery inflammation by 18F-fluorodeoxyglucose positron emission tomography in acute and chronic coronary artery disease. European Heart Journal Cardiovascular Imaging, 2021, 22, .	1.2	0
20	Seasonal Variation in the Brain μ-Opioid Receptor Availability. Journal of Neuroscience, 2021, 41, 1265-1273.	3.6	14
21	Comparison of: (2S,4R)-4-[18F]Fluoroglutamine, [11C]Methionine, and 2-Deoxy-2-[18F]Fluoro-D-Glucose and Two Small-Animal PET/CT Systems Imaging Rat Gliomas. Frontiers in Oncology, 2021, 11, 730358.	2.8	3
22	PET radiopharmaceuticals for imaging inflammatory diseases. , 2021, , .		0
23	Evaluation of [68Ca]Ga-NODAGA-RGD for PET Imaging of Rat Autoimmune Myocarditis. Frontiers in Medicine, 2021, 8, 783596.	2.6	2
24	Glucagon-like peptide-1 receptor expression after myocardial infarction: Imaging study using 68Ga-NODAGA-exendin-4 positron emission tomography. Journal of Nuclear Cardiology, 2020, 27, 2386-2397.	2.1	12
25	68Ga-DOTA chelate, a novel imaging agent for assessment of myocardial perfusion and infarction detection in a rodent model. Journal of Nuclear Cardiology, 2020, 27, 891-898.	2.1	10
26	Evaluation of cardiac function by nuclear imaging in preclinical studies. Journal of Nuclear Cardiology, 2020, 27, 1328-1330.	2.1	1
27	Hydroxysteroid (17β) dehydrogenase 12 is essential for metabolic homeostasis in adult mice. American Journal of Physiology - Endocrinology and Metabolism, 2020, 319, E494-E508.	3.5	12
28	Radiosynthesis and preclinical evaluation of [68Ga]Ga-NOTA-folate for PET imaging of folate receptor β-positive macrophages. Scientific Reports, 2020, 10, 13593.	3.3	10
29	Therapeutic Antibody Against Phosphorylcholine Preserves Coronary Function and Attenuates Vascular 18F-FDG Uptake in Atherosclerotic Mice. JACC Basic To Translational Science, 2020, 5, 360-373.	4.1	9
30	In Vivo Imaging of Inflammation and Infection 2019. Contrast Media and Molecular Imaging, 2020, 2020, 1-2.	0.8	1
31	Folate Receptor β–Targeted PET Imaging of Macrophages in Autoimmune Myocarditis. Journal of Nuclear Medicine, 2020, 61, 1643-1649.	5.0	31
32	Effects of dipeptidyl peptidase 4 inhibition on inflammation in atherosclerosis: A 18F-fluorodeoxyglucose study of a mouse model of atherosclerosis and type 2 diabetes. Atherosclerosis, 2020, 305, 64-72.	0.8	6
33	(2S, 4R)-4-[18F]Fluoroglutamine for In vivo PET Imaging of Glioma Xenografts in Mice: an Evaluation of Multiple Pharmacokinetic Models. Molecular Imaging and Biology, 2020, 22, 969-978.	2.6	16
34	Evaluation of image quality with four positron emitters and three preclinical PET/CT systems. EJNMMI Research, 2020, 10, 155.	2.5	12
35	245Evaluation of [18F]AlF-NOTA-Folate for PET imaging of rat autoimmune myocarditis. European Heart Journal Cardiovascular Imaging, 2019, 20, .	1.2	1
36	Fibroblast Growth Factor 21 Drives Dynamics of Local and Systemic Stress Responses in Mitochondrial Myopathy with mtDNA Deletions. Cell Metabolism, 2019, 30, 1040-1054.e7.	16.2	166

#	Article	IF	CITATIONS
37	The Clinical Impact of Using ¹⁸ F-FDG-PET/CT in the Diagnosis of Suspected Vasculitis: The Effect of Dose and Timing of Glucocorticoid Treatment. Contrast Media and Molecular Imaging, 2019, 2019, 1-8.	0.8	7
38	Mesenchymal Cell-Derived Juxtacrine Wnt1 Signaling Regulates Osteoblast Activity and Osteoclast Differentiation. Journal of Bone and Mineral Research, 2019, 34, 1129-1142.	2.8	29
39	Safety Study of Single-Dose Intravenously Administered DOTA-Siglec-9 Peptide in Sprague Dawley Rats. International Journal of Toxicology, 2019, 38, 4-11.	1.2	1
40	68Ga-DOTA-E[c(RGDfK)]2 PET Imaging of SHARPIN-Regulated Integrin Activity in Mice. Journal of Nuclear Medicine, 2019, 60, 1380-1387.	5.0	11
41	Noninvasive and Quantitative Monitoring of the Distributions and Kinetics of MicroRNA-Targeting Molecules in Vivo by Positron Emission Tomography. Molecular Pharmaceutics, 2019, 16, 1507-1515.	4.6	6
42	NEMA NU 4-2008 and <i>in vivo</i> imaging performance of RAYCAN trans-PET/CT X5 small animal imaging system. Physics in Medicine and Biology, 2019, 64, 115014.	3.0	8
43	Amyloid-Targeting PET Tracer [18F]Flutemetamol Accumulates in Atherosclerotic Plaques. Molecules, 2019, 24, 1072.	3.8	9
44	Kinetic Modelling of [68Ga]Ga-DOTA-Siglec-9 in Porcine Osteomyelitis and Soft Tissue Infections. Molecules, 2019, 24, 4094.	3.8	9
45	Folate receptor-targeted positron emission tomography of experimental autoimmune encephalomyelitis in rats. Journal of Neuroinflammation, 2019, 16, 252.	7.2	10
46	Determinants of Myocardial Strain in Experimental Chronic Myocardial Infarction. Ultrasound in Medicine and Biology, 2019, 45, 568-578.	1.5	3
47	Rapid spread of mannan to the immune system, skin and joints within 6 hours after local exposure. Clinical and Experimental Immunology, 2019, 196, 383-391.	2.6	7
48	Adventures in radiosynthesis of clinical grade [⁶⁸ Ga]Ga-DOTA-Siglec-9. RSC Advances, 2018, 8, 8051-8056.	3.6	5
49	<scp>PET</scp> / <scp>CT</scp> to detect adverse reactions to metal debris in patients with metalâ€onâ€metal hip arthroplasty: an exploratory prospective study. Clinical Physiology and Functional Imaging, 2018, 38, 847-855.	1.2	7
50	Morbid obesity and type 2 diabetes alter intestinal fatty acid uptake and blood flow. Diabetes, Obesity and Metabolism, 2018, 20, 1384-1390.	4.4	13
51	Vascular adhesion protein-1 is actively involved in the development of inflammatory lesions in rat models of multiple sclerosis. Journal of Neuroinflammation, 2018, 15, 128.	7.2	12
52	Evaluation of 68Ga-labeled peptide tracer for detection of gelatinase expression after myocardial infarction in rat. Journal of Nuclear Cardiology, 2018, 25, 1114-1123.	2.1	9
53	In vivo imaging of Lyme arthritis in mice by [¹⁸ F]fluorodeoxyglucose positron emission tomography/computed tomography. Scandinavian Journal of Rheumatology, 2018, 47, 37-47.	1.1	3
54	[P083] Kinetic modelling of [68Ga]Ga-DOTA-Siglec-9 in a porcine infection model. Physica Medica, 2018, 52, 124-125.	0.7	1

#	Article	IF	CITATIONS
55	Evaluation of [68Ga]Ga-DOTA-TCTP-1 for the Detection of Metalloproteinase 2/9 Expression in Mouse Atherosclerotic Plaques. Molecules, 2018, 23, 3168.	3.8	13
56	Positron Emission Tomography Imaging of Macrophages in Atherosclerosis with ¹⁸ F-GE-180, a Radiotracer for Translocator Protein (TSPO). Contrast Media and Molecular Imaging, 2018, 2018, 1-11.	0.8	27
57	Aluminum fluoride-18 labeled folate enables in vivo detection of atherosclerotic plaque inflammation by positron emission tomography. Scientific Reports, 2018, 8, 9720.	3.3	39
58	A Comparative ⁶⁸ Ga-Citrate and ⁶⁸ Ga-Chloride PET/CT Imaging of <i>Staphylococcus aureus</i> Osteomyelitis in the Rat Tibia. Contrast Media and Molecular Imaging, 2018, 2018, 1-10.	0.8	12
59	In Vivo Imaging of Inflammation and Infection. Contrast Media and Molecular Imaging, 2018, 2018, 1-2.	0.8	1
60	Exploring Alternative Radiolabeling Strategies for Sialic Acid-Binding Immunoglobulin-Like Lectin 9 Peptide: [68Ca]Ga- and [18F]AlF-NOTA-Siglec-9. Molecules, 2018, 23, 305.	3.8	7
61	Low STAT3 expression sensitizes to toxic effects of β-adrenergic receptor stimulation in peripartum cardiomyopathy. European Heart Journal, 2017, 38, ehw086.	2.2	87
62	18F-FDG positron emission tomography/computed tomography in infective endocarditis. Journal of Nuclear Cardiology, 2017, 24, 195-206.	2.1	64
63	Pretargeted PET Imaging of <i>trans</i> -Cyclooctene-Modified Porous Silicon Nanoparticles. ACS Omega, 2017, 2, 62-69.	3.5	50
64	Effects of atorvastatin and diet interventions on atherosclerotic plaque inflammation and [18F]FDG uptake in Ldlrâ^'/â^'Apob mice. Atherosclerosis, 2017, 263, 369-376.	0.8	18
65	Exploring the radiosynthesis and <i>in vitro</i> characteristics of [⁶⁸ Ga]Gaâ€DOTA‣iglecâ€9. Journal of Labelled Compounds and Radiopharmaceuticals, 2017, 60, 439-449.	1.0	12
66	In Vivo Imaging of Inflammation. , 2017, , 1567-1582.		0
67	Effects of linagliptin intervention on atherosclerotic plaque inflammation and 18F-FDG uptake in a mouse model of type 2 diabetes. Atherosclerosis, 2017, 263, e119-e120.	0.8	Ο
68	Positron emission tomography tracer [68GA]NODAGA-EXENDIN-4 detects glucagon-like peptide-1 receptor expression in mouse atherosclerotic vascular lesions. Atherosclerosis, 2017, 263, e55-e56.	0.8	1
69	Accuracy of echocardiographic area-length method in chronic myocardial infarction: comparison with cardiac CT in pigs. Cardiovascular Ultrasound, 2017, 15, 1.	1.6	12
70	lmaging of αvβ3 integrin expression in experimental myocardial ischemia with [68Ga]NODAGA-RGD positron emission tomography. Journal of Translational Medicine, 2017, 15, 144.	4.4	22
71	18-kDa translocator protein ligand 18F-FEMPA: Biodistribution and uptake into atherosclerotic plaques in mice. Journal of Nuclear Cardiology, 2017, 24, 862-871.	2.1	39
72	Comparison of 68Ga-DOTA-Siglec-9 and 18F-Fluorodeoxyribose-Siglec-9: Inflammation Imaging and Radiation Dosimetry. Contrast Media and Molecular Imaging, 2017, 2017, 1-10.	0.8	7

#	Article	IF	CITATIONS
73	Head-to-Head Comparison of68Ga-Citrate and18F-FDG PET/CT for Detection of Infectious Foci in Patients withStaphylococcus aureusBacteraemia. Contrast Media and Molecular Imaging, 2017, 2017, 1-8.	0.8	19
74	Targeting of vascular adhesion protein-1 by positron emission tomography visualizes sites of inflammation in Borrelia burgdorferi-infected mice. Arthritis Research and Therapy, 2017, 19, 254.	3.5	11
75	A Novel Positron Emission Tomography (PET) Approach to Monitor Cardiac Metabolic Pathway Remodeling in Response to Sunitinib Malate. PLoS ONE, 2017, 12, e0169964.	2.5	26
76	In Vivo Bone-Targeting of Bis(phosphonate)-Conjugated Double Helical RNA Monitored by Positron Emission Tomography. Molecular Pharmaceutics, 2016, 13, 2588-2595.	4.6	8
77	Influence of triple disease modifying anti-rheumatic drug therapy on carotid artery inflammation in drug-naive patients with recent onset of rheumatoid arthritis. Rheumatology, 2016, 55, 1777-1785.	1.9	10
78	Leukocyte trafficking-associated vascular adhesion protein 1 is expressed and functionally active in atherosclerotic plaques. Scientific Reports, 2016, 6, 35089.	3.3	30
79	Type 2 diabetes enhances arterial uptake of choline in atherosclerotic mice: an imaging study with positron emission tomography tracer 18F-fluoromethylcholine. Cardiovascular Diabetology, 2016, 15, 26.	6.8	27
80	18F-Labeling of Mannan for Inflammation Research with Positron Emission Tomography. ACS Medicinal Chemistry Letters, 2016, 7, 826-830.	2.8	11
81	USF1 deficiency activates brown adipose tissue and improves cardiometabolic health. Science Translational Medicine, 2016, 8, 323ra13.	12.4	58
82	Effect of levosimendan therapy on myocardial infarct size and left ventricular function after acute coronary occlusion. Heart, 2016, 102, 465-471.	2.9	7
83	Mitochondrial DNA Replication Defects Disturb Cellular dNTP Pools and Remodel One-Carbon Metabolism. Cell Metabolism, 2016, 23, 635-648.	16.2	222
84	Synthesis and In Vivo PET Imaging of Hyaluronan Conjugates of Oligonucleotides. Bioconjugate Chemistry, 2016, 27, 391-403.	3.6	16
85	Comparison of Somatostatin Receptor 2-Targeting PET Tracers in the Detection of Mouse Atherosclerotic Plaques. Molecular Imaging and Biology, 2016, 18, 99-108.	2.6	48
86	Feasibility of (68)Ga-labeled Siglec-9 peptide for the imaging of acute lung inflammation: a pilot study in a porcine model of acute respiratory distress syndrome. American Journal of Nuclear Medicine and Molecular Imaging, 2016, 6, 18-31.	1.0	16
87	68Ga-DOTA-Siglec-9 – a new imaging tool to detect synovitis. Arthritis Research and Therapy, 2015, 17, 308.	3.5	31
88	[18F]FDG Accumulation in Early Coronary Atherosclerotic Lesions in Pigs. PLoS ONE, 2015, 10, e0131332.	2.5	5
89	Enabling [¹⁸ F]-bicyclo[6.1.0]nonyne for oligonucleotide conjugation for positron emission tomography applications: [¹⁸ F]-anti-microRNA-21 as an example. Chemical Communications, 2015, 51, 9821-9824.	4.1	16
90	Somatostatin receptor subtype 2 in high-grade gliomas: PET/CT with 68Ga-DOTA-peptides, correlation to prognostic markers, and implications for targeted radiotherapy. EJNMMI Research, 2015, 5, 25.	2.5	20

#	Article	IF	CITATIONS
91	Test–retest reliability of 11C-ORM-13070 in PET imaging of α2C-adrenoceptors in vivo in the human brain. European Journal of Nuclear Medicine and Molecular Imaging, 2015, 42, 120-127.	6.4	130
92	Cardiac remodeling in a new pig model of chronic heart failure: Assessment of left ventricular functional, metabolic, and structural changes using PET, CT, and echocardiography. Journal of Nuclear Cardiology, 2015, 22, 655-665.	2.1	19
93	Absorption, distribution and excretion of intravenously injected 68Ge/68Ga generator eluate in healthy rats, and estimation of human radiation dosimetry. EJNMMI Research, 2015, 5, 117.	2.5	20
94	Abstract 18873: Al ¹⁸ F-NOTA-folate Accumulates in Atherosclerotic Plaques and Can be Detected by PET/CT. Circulation, 2015, 132, .	1.6	0
95	Pancreatic Metabolism, Blood Flow, and β-Cell Function in Obese Humans. Journal of Clinical Endocrinology and Metabolism, 2014, 99, E981-E990.	3.6	33
96	Widespread vascular inflammation in a patient with antineutrophil cytoplasmic antibody-associated vasculitis as detected by positron emission tomography. European Journal of Nuclear Medicine and Molecular Imaging, 2014, 41, 2167-2168.	6.4	2
97	Feasibility of experimental BT4C glioma models for somatostatin receptor 2-targeted therapies. Acta Oncológica, 2014, 53, 1125-1134.	1.8	5
98	Synthesis of multi-galactose-conjugated 2′-O-methyl oligoribonucleotides and their in vivo imaging with positron emission tomography. Bioorganic and Medicinal Chemistry, 2014, 22, 6806-6813.	3.0	16
99	[¹⁸ F]Fluorodeoxyglucose Uptake in Atherosclerotic Plaques Is Associated With Reduced Coronary Flow Reserve in Mice. Journal of Ultrasound in Medicine, 2014, 33, 1941-1948.	1.7	1
100	Dimeric [68Ga]DOTA-RGD Peptide Targeting αvβ3 Integrin Reveals Extracellular Matrix Alterations after Myocardial Infarction. Molecular Imaging and Biology, 2014, 16, 793-801.	2.6	26
101	Use of a clinical PET/MR scanner for preclinical research with first results. EJNMMI Physics, 2014, 1, A88.	2.7	0
102	68Ca-DOTA-Siglec-9 PET/CT imaging of peri-implant tissue responses and staphylococcal infections. EJNMMI Research, 2014, 4, 45.	2.5	21
103	11C-ORM-13070, a novel PET ligand for brain α2C-adrenoceptors: radiometabolism, plasma pharmacokinetics, whole-body distribution and radiation dosimetry in healthy men. European Journal of Nuclear Medicine and Molecular Imaging, 2014, 41, 1947-1956.	6.4	16
104	64Cu- and 68Ga-Labelled [Nle14,Lys40(Ahx-NODAGA)NH2]-Exendin-4 for Pancreatic Beta Cell Imaging in Rats. Molecular Imaging and Biology, 2014, 16, 255-263.	2.6	55
105	Pharmacological Activation of the Melanocortin System Limits Plaque Inflammation and Ameliorates Vascular Dysfunction in Atherosclerotic Mice. Arteriosclerosis, Thrombosis, and Vascular Biology, 2014, 34, 1346-1354.	2.4	21
106	Using 5-deoxy-5-[18F]fluororibose to glycosylate peptides for positron emission tomography. Nature Protocols, 2014, 9, 138-145.	12.0	22
107	Cardiac hypertrophy and oxidative metabolism in novel congenic leptin receptor deficient BBDR.cgâ€lepr.cp rats (1155.10). FASEB Journal, 2014, 28, 1155.10.	0.5	1
108	Assessment of blood flow with (68)Ga-DOTA PET in experimental inflammation: a validation study using (15)O-water. American Journal of Nuclear Medicine and Molecular Imaging, 2014, 4, 571-9.	1.0	9

#	Article	IF	CITATIONS
109	Characterization of hepatic tumors using [11C]metomidate through positron emission tomography: comparison with [11C]acetate. EJNMMI Research, 2013, 3, 13.	2.5	5
110	Nuclear imaging of inflammation: homing-associated molecules as targets. EJNMMI Research, 2013, 3, 1.	2.5	75
111	Correlation of 18F-FDG PET/CT assessments with disease activity and markers of inflammation in patients with early rheumatoid arthritis following the initiation of combination therapy with triple oral antirheumatic drugs. European Journal of Nuclear Medicine and Molecular Imaging, 2013, 40, 403-410.	6.4	66
112	Translating the concept of peptidelabeling with 5-deoxy-5-[¹⁸ F]fluororibose into preclinical practice: ¹⁸ F-labeling of Siglec-9 peptide for PET imaging of inflammation. Chemical Communications, 2013, 49, 3682-3684.	4.1	33
113	Synthesis and preclinical characterization of [64Cu]NODAGA-MAL-exendin-4 with a Nlµ-maleoyl-l-lysyl-glycine linkage. Nuclear Medicine and Biology, 2013, 40, 1006-1012.	0.6	23
114	Preclinical Evaluation of a Radioiodinated Fully Human Antibody for In Vivo Imaging of Vascular Adhesion Protein-1–Positive Vasculature in Inflammation. Journal of Nuclear Medicine, 2013, 54, 1315-1319.	5.0	22
115	Plasma Pharmacokinetics, Whole-Body Distribution, Metabolism, and Radiation Dosimetry of ⁶⁸ Ga Bombesin Antagonist BAY 86-7548 in Healthy Men. Journal of Nuclear Medicine, 2013, 54, 867-872.	5.0	93
116	<i>In Vivo</i> Imaging of Prostate Cancer Using [68Ga]-Labeled Bombesin Analog BAY86-7548. Clinical Cancer Research, 2013, 19, 5434-5443.	7.0	174
117	[¹⁸ F]-Fluorodeoxyglucose Positron Emission Tomography and Computed Tomography in Response Evaluation of Oncolytic Adenovirus Treatments of Patients with Advanced Cancer. Human Gene Therapy, 2013, 24, 1029-1041.	2.7	23
118	Celiac Disease–Specific TG2-Targeted Autoantibodies Inhibit Angiogenesis Ex Vivo and In Vivo in Mice by Interfering with Endothelial Cell Dynamics. PLoS ONE, 2013, 8, e65887.	2.5	22
119	Evaluation of 68Ga-labeled tracers for PET imaging of myocardial perfusion in pigs. Nuclear Medicine and Biology, 2012, 39, 715-723.	0.6	20
120	Solid-Supported NOTA and DOTA Chelators Useful for the Synthesis of 3â€2-Radiometalated Oligonucleotides. Bioconjugate Chemistry, 2012, 23, 1981-1988.	3.6	18
121	A comparative 18F-FDG PET/CT imaging of experimental Staphylococcus aureus osteomyelitis and Staphylococcus epidermidis foreign-body-associated infection in the rabbit tibia. EJNMMI Research, 2012, 2, 41.	2.5	28
122	Cross-validation of Input Functions Obtained by H2 15O PET Imaging of Rat Heart and a Blood Flow-through Detector. Molecular Imaging and Biology, 2012, 14, 509-516.	2.6	9
123	Gallium-labelled peptides for imaging of inflammation. European Journal of Nuclear Medicine and Molecular Imaging, 2012, 39, 68-77.	6.4	38
124	Effects of Age, Diet, and Type 2 Diabetes on the Development and FDG Uptake of Atherosclerotic Plaques. JACC: Cardiovascular Imaging, 2011, 4, 1294-1301.	5.3	41
125	Siglec-9 is a novel leukocyte ligand for vascular adhesion protein-1 and can be used in PET imaging of inflammation and cancer. Blood, 2011, 118, 3725-3733.	1.4	100
126	Mini-PEG spacering of VAP-1-targeting 68Ga-DOTAVAP-P1 peptide improves PET imaging of inflammation. EJNMMI Research, 2011, 1, 10.	2.5	30

#	Article	IF	CITATIONS
127	Uptake of 68gallium in atherosclerotic plaques in LDLR-/-ApoB100/100 mice. EJNMMI Research, 2011, 1, 14.	2.5	26
128	Extraction of Input Function from Rat [18F]FDG PET Images. Molecular Imaging and Biology, 2011, 13, 1241-1249.	2.6	7
129	Detection of Hypoxia by [¹⁸ F]EF5 in Atherosclerotic Plaques in Mice. Arteriosclerosis, Thrombosis, and Vascular Biology, 2011, 31, 1011-1015.	2.4	36
130	Measurements of [¹¹ C]CO <inf>2</inf> in exhaled air with a positron-sensitive single-wire proportional counter after i.v. injection of [¹¹ C]acetate. , 2011, , .		0
131	Imaging of Insulitis in NOD Mice with IL-2-Gd-DTPA and 1.5 T MRI. Advances in Molecular Imaging, 2011, 01, 43-49.	0.3	2
132	Human Subject with Unexpected Biodistribution of [11C]PK11195. The Open Nuclear Medicine Journal, 2011, 3, 10-11.	0.2	0
133	Human biodistribution and radiation dosimetry of 11C-(R)-PK11195, the prototypic PET ligand to image inflammation. European Journal of Nuclear Medicine and Molecular Imaging, 2010, 37, 606-612.	6.4	39
134	Biodistribution and radiation dosimetry of [11C]choline: a comparison between rat and human data. European Journal of Nuclear Medicine and Molecular Imaging, 2010, 37, 874-883.	6.4	54
135	PET imaging of inflammation and adenocarcinoma xenografts using vascular adhesion protein 1 targeting peptide 68Ga-DOTAVAP-P1: comparison with 18F-FDG. European Journal of Nuclear Medicine and Molecular Imaging, 2010, 37, 1918-1925.	6.4	31
136	68Ga-Chloride PET Reveals Human Pancreatic Adenocarcinoma Xenografts in Rats—Comparison with FDG. Molecular Imaging and Biology, 2010, 12, 259-268.	2.6	14
137	Human Dosimetry of Carbon-11 Labeled N-butan-2-yl-1-(2-chlorophenyl)-N-methylisoquinoline-3-carboxamide Extrapolated from Whole-body Distribution Kinetics and Radiometabolism in Rats. Molecular Imaging and Biology, 2010, 12, 435-442.	2.6	9
138	Preliminary evaluation of novel68Ga-DOTAVAP-PEG-P2 peptide targeting vascular adhesion protein-1. Clinical Physiology and Functional Imaging, 2010, 30, 75-78.	1.2	17
139	A multi-wire proportional counter for measurement of positron-emitting radionuclides during on-line blood sampling. , 2010, , .		1
140	Uptake of ¹¹ C-Choline in Mouse Atherosclerotic Plaques. Journal of Nuclear Medicine, 2010, 51, 798-802.	5.0	53
141	Fatty Acid Metabolism in the Liver, Measured by Positron Emission Tomography, Is Increased in Obese Individuals. Gastroenterology, 2010, 139, 846-856.e6.	1.3	144
142	Matrix Metalloproteinase 9 Targeting Peptides: Syntheses, ⁶⁸ Ga-labeling, and Preliminary Evaluation in a Rat Melanoma Xenograft Model. Bioconjugate Chemistry, 2010, 21, 1612-1621.	3.6	28
143	Uptake of inflammatory cell marker [11C]PK11195 into mouse atherosclerotic plaques. European Journal of Nuclear Medicine and Molecular Imaging, 2009, 36, 73-80.	6.4	48
144	Whole-body distribution and metabolism of [N-methyl-11C](R)-1-(2-chlorophenyl)-N-(1-methylpropyl)-3-isoquinolinecarboxamide in humans; an imaging agent for in vivo assessment of peripheral benzodiazepine receptor activity with positron emission tomography. European Journal of Nuclear Medicine and Molecular Imaging, 2009, 36, 671-682.	6.4	40

#	Article	IF	CITATIONS
145	68Ga-DOTA-RGD peptide: biodistribution and binding into atherosclerotic plaques in mice. European Journal of Nuclear Medicine and Molecular Imaging, 2009, 36, 2058-2067.	6.4	57
146	Synthesis, 68Ga labeling and preliminary evaluation of DOTA peptide binding vascular adhesion protein-1: a potential PET imaging agent for diagnosing osteomyelitis. Nuclear Medicine and Biology, 2009, 36, 631-641.	0.6	40
147	68Ga-DOTAVAP-P1 PET imaging capable of demonstrating the phase of inflammation in healing bones and the progress of infection in osteomyelitic bones. European Journal of Nuclear Medicine and Molecular Imaging, 2008, 35, 352-364.	6.4	47
148	Measurement of Striatal and Extrastriatal Dopamine Transporter Binding with High-Resolution PET and [¹¹ C]PE2I: Quantitative Modeling and Test—Retest Reproducibility. Journal of Cerebral Blood Flow and Metabolism, 2008, 28, 1059-1069.	4.3	63
149	1- ¹¹ C-Methyl-4-Piperidinyl- <i>N</i> Butyrate Radiation Dosimetry in Humans by Dynamic Organ-Specific Evaluation. Journal of Nuclear Medicine, 2008, 49, 347-353.	5.0	12
150	Pancreatic Glucose Uptakein Vivoin Men with Newly Diagnosed Type 1 Diabetes. Journal of Clinical Endocrinology and Metabolism, 2008, 93, 1909-1914.	3.6	8
151	Non-specific binding of [18F]FDG to calcifications in atherosclerotic plaques: experimental study of mouse and human arteries. European Journal of Nuclear Medicine and Molecular Imaging, 2006, 33, 1461-1467.	6.4	40
152	Whole-body distribution of 11C-choline and uptake in knee synovitis. European Journal of Nuclear Medicine and Molecular Imaging, 2006, 33, 1372-1373.	6.4	18
153	Biodistribution of 68Ga-labelled phosphodiester, phosphorothioate, and 2′-O-methyl phosphodiester oligonucleotides in normal rats. European Journal of Pharmaceutical Sciences, 2005, 26, 26-38.	4.0	57
154	Comparison of 18F-FDG and 68Ga PET imaging in the assessment of experimental osteomyelitis due to Staphylococcus aureus. European Journal of Nuclear Medicine and Molecular Imaging, 2005, 32, 1259-1268.	6.4	69
155	Kinetics of [11 C]choline uptake in prostate cancer: a PET stydy. European Journal of Nuclear Medicine and Molecular Imaging, 2004, 31, 317-324.	6.4	181
156	68Ca-labeled oligonucleotides for in vivo imaging with PET. Journal of Nuclear Medicine, 2004, 45, 347-55.	5.0	71
157	Imaging of adrenal incidentalomas with PET using (11)C-metomidate and (18)F-FDG. Journal of Nuclear Medicine, 2004, 45, 972-9.	5.0	76
158	Biodistribution and blood metabolism of 1-11C-methyl-4-piperidinyl n-butyrate in humans: an imaging agent for in vivo assessment of butyrylcholinesterase activity with PET. Journal of Nuclear Medicine, 2004, 45, 2032-9.	5.0	18
159	Quantifying tumour hypoxia with fluorine-18 fluoroerythronitroimidazole ([18 F]FETNIM) and PET using the tumour to plasma ratio. European Journal of Nuclear Medicine and Molecular Imaging, 2003, 30, 101-108.	6.4	76
160	Use of positron emission tomography with methyl-11C-choline and 2-18F-fluoro-2-deoxy-D-glucose in comparison with magnetic resonance imaging for the assessment of inflammatory proliferation of synovium. Arthritis and Rheumatism, 2003, 48, 3077-3084.	6.7	107
161	Regional Effects of Donepezil and Rivastigmine on Cortical Acetylcholinesterase Activity in Alzheimer's Disease. Journal of Clinical Psychopharmacology, 2002, 22, 615-620.	1.4	122
162	Blood metabolism of [methyl- 11C]choline; implications for in vivo imaging with positron emission tomography. European Journal of Nuclear Medicine and Molecular Imaging, 2000, 27, 25-32.	2.1	121

#	Article	IF	CITATIONS
163	H-ras oncogene point mutations in arthritic synovium. Arthritis and Rheumatism, 1997, 40, 1636-1643.	6.7	68
164	[68Ga]Ga-DOTA-Siglec-9 Detects Pharmacodynamic Changes of FAP-Targeted IL2 Variant Immunotherapy in B16-FAP Melanoma Mice. Frontiers in Immunology, 0, 13, .	4.8	1